https://doi.org/10.5194/egusphere-2023-835
Preprint. Discussion started: 24 May 2023

The application and modification of WRF-Hydro/Glacier to a cold-based Antarctic glacier

Tamara Pletzer[1], Jonathan P. Conway[2], Nicolas J. Cullen[1], Trude Eidhammer[3], and Marwan Katurji[4]

[1]School of Geography, University of Otago, Ōtepoti/Dunedin, New Zealand
[2] National Institute of Water and Atmospheric Research, Lauder, New Zealand
[3]National Center for Atmospheric Research, P.O. Box 3000, Boulder, CO 80307, USA
[4]School of Earth and Environment, University of Canterbury, Ōtautahi/Christchurch, New Zealand

Correspondence: Tamara Pletzer (tamara.pletzer@postgrad.otago.ac.nz)

Abstract. The McMurdo Dry Valleys (MDV) are home to a unique microbial ecosystem dependent on the availability of freshwater. It is a polar desert and freshwater originates almost entirely from surface and near-surface melt of cold-based glaciers. Understanding the future evolution of these environments requires the simulation of the full chain of physical processes-from net radiative forcing, surface energy balance, melt, runoff and the transport of meltwater in stream channels from the glaciers to the terminal lakes where the microbial community resides. We present the first application of the WRF-Hydro/Glacier model in the MDV. The model was tested for a 7-month period (1 August 2021 to 28 February 2022) at a point on Commonwealth Glacier and forced by automatic weather station observations. We found it was necessary to limit the percolation of meltwater through ice layers to represent near-surface runoff as observed in the field. We also tuned the parameters controlling the spectral albedo for snow and ice based on observations to model the evolution of broadband albedo over a melt season. With these modifications, we were able to accurately simulate surface and near-surface temperatures, surface height change, broadband albedo and runoff over a melt season. These modifications show that once the model is adapted to this extreme environment, the model is capable of accurately capturing the physical processes governing the meltwater generation of an MDV glacier. This will enable future efforts to model spatially distributed melt and streamflow in the MDV and will allow us to answer questions around the timing of meltwater transport and the present and future hydrological response of melt to atmospheric forcing.

1 Introduction

Glaciers are the largest store of freshwater on the planet. Glacial melt provides water in dry seasons and in arid climates. The McMurdo Dry Valleys (MDV) are no exception as a polar desert where freshwater in the lakes and streams originates almost entirely from glacial melt. There is a unique microbial ecosystem that resides in the streams and lakes and is dependent on glacial meltwater (Gooseff et al., 2011). It is expected that the biogeography of this ecosystem will be altered in response to future changes in climate, thus it is key to understand and simulate the hydrological connectivity of meltwater.

https://doi.org/10.5194/egusphere-2023-835
Preprint. Discussion started: 24 May 2023

Unlike most mid-latitude glaciers, the glaciers in the MDV are mainly cold-based, meaning that the subsurface temperatures are below the pressure melting point and ice is frozen to the bedrock (Fitzsimons, 1996; Gooseff et al., 2011; Fountain et al., 2016). Glacial melt is driven by solar radiation and small changes in energy (for example, through albedo) can have a large impact on melt generation (Hoffman et al., 2008; Macdonell et al., 2013). Solar radiation penetrates the top 5-15 cm of the glacier (Hoffman et al., 2014) and this near-surface layer can retain heat longer than the surface due to the solid state greenhouse effect (Brandt and Warren, 1993). This effect extends the duration of melt events and modelling studies suggest melt from this layer is an order of magnitude larger than surface melt (Hoffman et al., 2014). Meltwater can percolate, refreeze, evaporate if at the surface, be stored on glacier (e.g. in snowpack, cryoconite holes or ponds) or runoff in surface and near-surface channels (MacDonell, 2008). Runoff then flows off-glacier and from there can be absorbed in the ground, evaporate, freeze or flow overland in the streams to terminate in one of the basin lakes or flow into McMurdo Sound.

MacDonell (2008) was the first to study the full hydrological drainage system and developed a conceptual modelling framework for cold-based glacial meltwater drainage processes on Lower Wright Glacier in Wright Valley. This study identified the need for a physically based, rather than empirical, model to simulate the complex drainage systems of MDV glaciers and the lack of such a model at that time (MacDonell, 2008). Hoffman (2011) was the first to implement a distributed surface energy balance model and investigated the spatial distribution of glacial melt over different catchments in Taylor Valley. This study showed that albedo, shortwave penetrative radiation and meltwater drainage were all important for accurately modelling the observed surface ablation (Hoffman, 2011). Cross et al. (2022) extended this work by coupling the glacial energy balance model used by Hoffman (2011) with a lake energy balance model to model the lake sublimation and water budget. Whilst both Hoffman (2011) and Cross et al. (2022) model glacial runoff, neither explicitly model the off-glacier processes in the hydrological system, such as streams or soil moisture.

The WRF-Hydro/Glacier model (Gochis et al., 2020; Eidhammer et al., 2021) provides an opportunity to fill this gap in hydrological connectivity due to its ability to physically model the full hydrological cycle between the atmosphere, glacier, bare ground land surface, stream channels and terminal lakes. WRF-Hydro/Glacier contains a detailed snowpack model (Crocus) embedded within a distributed hydrological model (WRF-Hydro) and is flexible enough to simulate the exchanges of moisture and energy between these different parts of the water budget. Eidhammer et al. (2021) implemented WRF-Hydro/Glacier on a temperate Norwegian glacier and demonstrated that it accurately simulated the mass balance, snow depth, surface albedo and runoff when compared to observations. However, the hydrology of a cold-based MDV glacier is significantly different (MacDonell, 2008). Therefore, further testing is required to implement WRF-Hydro/Glacier in this environment.

This study aims to adapt WRF-Hydro/Glacier to simulate surface and near-surface runoff from a glacier in the MDV. WRF-Hydro/Glacier is implemented at a point on Commonwealth Glacier forced by automatic weather station data and tested against observations of broadband albedo, surface and near-surface ice temperatures, surface height change and streamflow. Given that it is the first time this model has been implemented in a polar region and on a cold-based glacier, it was necessary to modify

https://doi.org/10.5194/egusphere-2023-835
Preprint. Discussion started: 24 May 2023

several model schemes, notably the calculations for percolation of water through the glacier and the spectral albedo scheme. These modifications will enable future efforts to model the full hydrological connectivity of glacial meltwater within the MDV.

The next section describes the WRF-Hydro/Glacier model set up and initialization. Section 3 describes the site and the data used to force and validate the model. Section 4 details the modifications to the Crocus snowpack meltwater drainage and spectral albedo schemes necessary to adapt the model to a cold-based glacial environment. Section 5 compares the performance of the original and modified versions of the model to observational data over the 2021/22 melt season.

2 Model Description

2.1 WRF-Hydro/Glacier

WRF-Hydro V5.2.0 is a multi-scale and spatially distributed hydro-meteorological modelling system developed by NCAR (Gochis et al., 2020). The model links a column land surface model (NoahMP) with subsurface flow, routing, overland flow, channel routing and water management modules (i.e. reservoir). It can be either forced by meteorological data in standalone mode or has the capability to run coupled atmosphere-hydrology simulations. WRF-Hydro is currently the National Water Model in the contiguous USA. It has applications from flood forecasting to regional hydroclimate impact assessments and has been validated extensively across six continents (e.g. (Senatore et al., 2015; Li et al., 2017; Xiang et al., 2017; Kerandi et al., 2018; Lahmers et al., 2021; Pal et al., 2021)). More recently, Eidhammer et al. (2021) developed the WRF-Hydro/Glacier model by coupling the detailed Crocus snowpack model to the NoahMP land surface model in order to simulate the energy and mass balance over glacial surfaces. The snow module in NoahMP does not allow the glacier to decrease in mass once the snow layers are melted because it represents the glacier as a bare ice land surface category with constant albedo, roughness length and heat conductivity. This representation does not allow melt and thus, was not sufficient to model glacial melt and runoff (Eidhammer et al., 2021).

Crocus is a detailed column snowpack model that was developed initially for avalanche forecasting in Col de Porte, France by MeteoFrance (Brun et al., 1992). The model version implemented in WRF-Hydro/Glacier is described in Vionnet et al. (2012). This version was chosen by Eidhammer et al. (2021) due to extensive validation and suitability for coupling to the NoahMP land surface scheme. The model physics include schemes for snow metamorphism, compaction, albedo, penetrating solar radiation, energy balance fluxes, heat diffusion, melt, refreezing, percolation, runoff and sublimation/deposition. Crocus simulates state variables in layers: heat content, thickness, density, age, history of snow and two snow grain properties that describe the dendricity, sphericity and grain size of the snow or ice crystals over a prescribed number of layers. All other variables such as snow temperature and liquid water content are calculated from the state variables. Further information can be found in Vionnet et al. (2012) and Eidhammer et al. (2021).

https://doi.org/10.5194/egusphere-2023-835
Preprint. Discussion started: 24 May 2023

3 Methods and Data

3.1 Site Description

Commonwealth Glacier is located on the eastern side of Taylor Valley approximately 4 km from McMurdo Sound (Fig. 1). It is a piedmont glacier, terminating in cliffs and is characterized by a smooth surface. The mean annual temperature from 1986–2017 is -17.6 °C, however in the summer temperatures can reach a maximum of 7.8 °C and in winter the temperature can descend to a minimum of -45.0 °C (Obryk et al., 2020). The wind directions are characterized by a bimodal distribution in the summer, mainly a daytime easterly sea breeze coming from McMurdo Sound and northerly down-glacier wind due to the low sun angle and the temperature differences between the glacier and bare ground on the valley floor at night time (Fountain and Doran, 2004). In the winter, this down-glacier wind becomes more persistent as the ice cools faster than the bare ground. There is also a low frequency westerly in both summer and winter that is a down-valley wind (Nylen et al., 2004). The down valley winds can either be a föhn wind from a synoptic cyclone or a katabatic descending from the Antarctic Plateau (Speirs et al., 2010; Steinhoff et al., 2013). Wind speeds on average are 2.2 m s^{-1}, with the strongest reported reaching a maximum of 44.5 m s^{-1} (Obryk et al., 2020).

3.2 Automatic Weather Stations

Data from two automatic weather stations (AWSs) are used in this study. The CWG AWS was installed on 1 December 2021 and is used for tuning and validation. It is located at $-77.56485°$, $163.2776°$ at 280 meters in elevation. CWG AWS measures air temperature, relative humidity, wind speed and direction, air pressure, near-surface ice temperatures and the incoming and outgoing components of shortwave and longwave radiation (Fig. 1). Table 1 shows the instruments and accuracy of each sensor. The instruments are sampled every 1 minute and averages are taken every 30 minutes. Data are stored on a CR1000 data logger.

For the model spin-up, the MDV Long Term Ecological Research Project station on Commonwealth Glacier (COHM AWS) (Doran and Fountain, 2022) is used because it is before the CWG AWS was installed. The COHM AWS is located 140 m east of CWG AWS at $-77.563712°$, $163.280145°$ and 290 m in elevation. The instruments and accuracy are detailed in Gooseff et al. (2022).

3.3 Model forcing

The model is forced at an hourly time step by observational data from the COHM AWS and CWG AWS. The following meteorological variables were used: incoming shortwave radiation (W m^{-2}), incoming longwave radiation (W m^{-2}), air temperature at 2 meters (K), the meridional and zonal wind vector components (m s^{-1}), specific humidity (kg kg^{-1}), pressure (hPa) and precipitation (mm water-equivalent s^{-1}). The data from the AWSs were processed similarly to Gillett and Cullen (2011), where specific humidity was calculated with respect to water and ice depending on whether the air temperature was above the melting

https://doi.org/10.5194/egusphere-2023-835
Preprint. Discussion started: 24 May 2023

Table 1. Variables and instruments on CWG AWS installed on 1 December 2021. The instruments sample every 1 minute and averages are taken every 30 minutes. Data is stored on a CR1000 data logger. Radiation accuracies for shortwave and longwave radiation are given in terms of the estimated accuracy of daily totals (EADT).

Variable	Instrument	Accuracy	Sensor height (m)
Wind speed	Young Wind Anemometer 05108-L40	± 0.3 m s^{-1} or 1 %	2.3
Wind direction	Young Wind Anemometer 05108-L40	± 3.0 °	2.3
Air temperature	Vaisala HMP 155	± 0.17 °C at 20 °C	1.4
Relative humidity	Vaisala HMP 155	± 1 (%RH 0-90) at 20 °C ± 1.7 (%RH 90-100) at 20 °C	1.4
Ice temperature	Type T Thermocouples	± 1 °C or 0.75%	-0.05, -0.1, -0.2, -0.5, -1.0 and -2.0 (initial heights)
Shortwave radiation (incoming and outgoing)	Apogee Pyranometer SN500SS	< 5 % EADT	1.8
Longwave radiation (incoming and outgoing)	Apogee Pyranometer SN500SS	± 5 % EADT	1.8
Distance to surface	SR50 Sonic ranger	± 1 cm or 0.4 % of distance to target	1.7
Pressure	Vaisala PTB110	± 0.3 hPa at 20 °C	0.5

point. The data for the model spin-up was obtained from the COHM AWS as it was for the period before the CWG AWS was installed (Doran and Fountain, 2022). Pressure for the spin-up period was obtained from the nearest grid cell to the CWG AWS in Antarctic Mesoscale WRF Prediction System (AMPS) atmospheric data as there was no barometer on the COHM AWS.

Given that there was no precipitation sensor on either AWS, precipitation was obtained using changes in snow height measurements from the SR50 sensor on COHM and CWG AWSs. Fountain et al. (2010) calculated precipitation in the MDV by taking the daily average change in snow height. If the change in snow height between days was greater than 5 mm, this was taken as precipitation. We attempted this method by Fountain et al. (2010), but found that it filtered out all of the summer snowfall events (some of which were witnessed during field work). Instead, we opted to fit a K nearest neighbors regression (n=30 and uniform weights) to the 30 minute snow height timeseries in order to filter the noise from the sensor. This method is similar to a rolling mean and smooths the snow height timeseries. Values below 0.3 mm (0.4 mm for January and February) of change in snow height during a 30 minute period were removed to filter noise from the sensor. This threshold was tuned to observations of snow events from the 2021/22 field campaign and observed albedo. Next, the positive increases in the hourly sum of surface height change were converted to mm water-equivalent using a fresh snow density of 150 kg m^{-3} to convert height change to the mass of snow.

https://doi.org/10.5194/egusphere-2023-835
Preprint. Discussion started: 24 May 2023

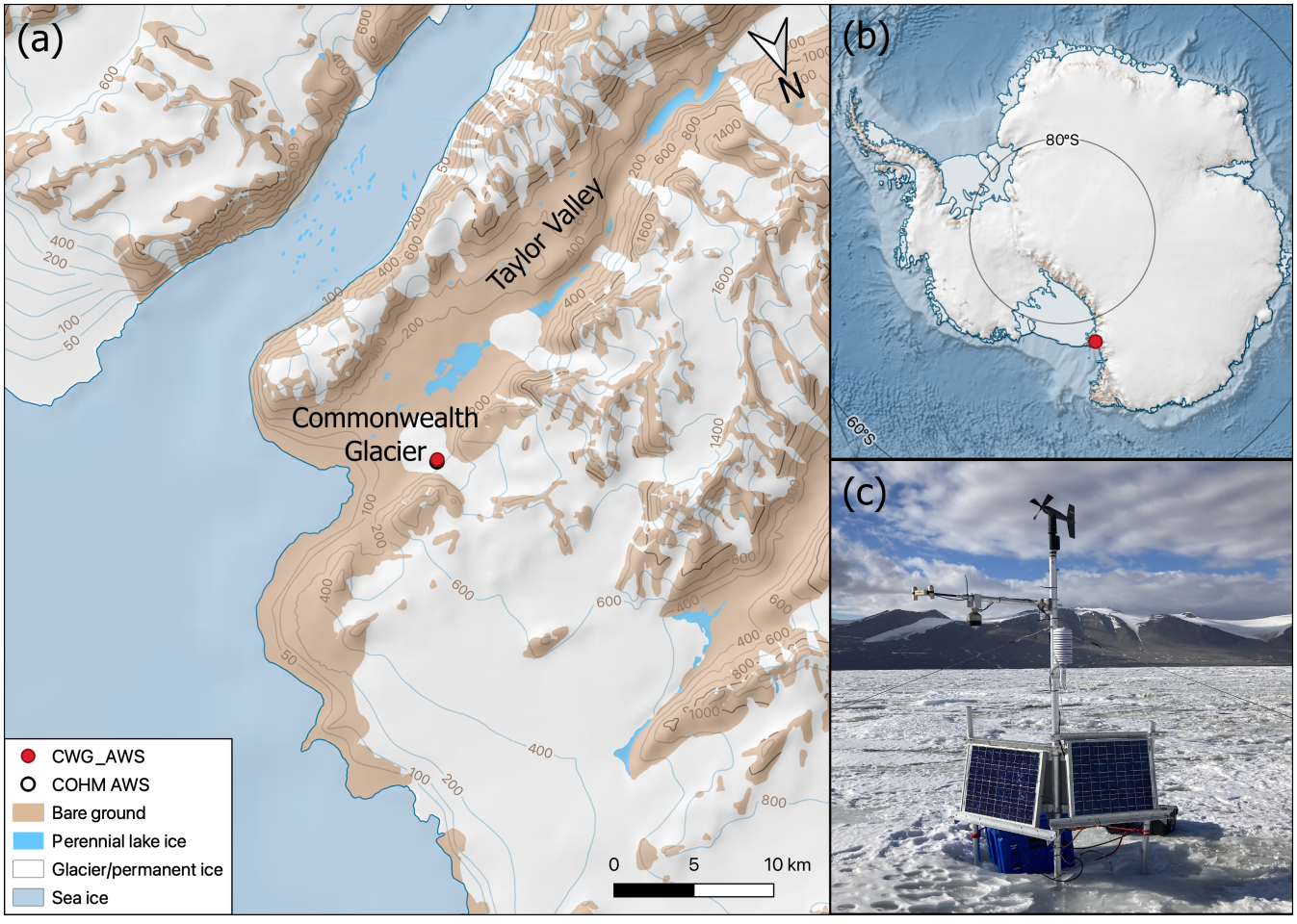

Figure 1. (a) Map of Commonwealth Glacier with respect to Taylor Valley with the CWG AWS in red filled circle and the COHM AWS indicated by a black open circle located 140 meters to the west of the COHM AWS. (b) Taylor Valley with respect to the continent. (c) The CWG AWS on 31 January 2022. Detailed basemaps from RAMP2 Hillshade, ETOPO1/IBCSCO/RAMP2 Hillshade and Elevation model. This map was made using the Quantarctica QGIS package collated by the Norwegian Polar Institute (https://www.npolar.no/quantarctica/, last access: 9 April 2023).

The forcing data are displayed in Fig. 2. Meteorological conditions vary seasonally with a stark difference in incoming shortwave radiation between the polar night and summer. This controls the surface temperatures that vary between the melting point in the summer and a minimum of -43 °C in August, which is often the coldest month in the MDV. Relative humidities are low and snowfall amounts are very low, with a higher frequency near the end of the summer season. Wind direction varies between northeasterlies (sea breeze), northerlies (down glacier katabatic) and westerlies (föhn), with the greatest wind speeds occurring when there is a westerly. The average pressure over the period is 950 hPa.

https://doi.org/10.5194/egusphere-2023-835
Preprint. Discussion started: 24 May 2023

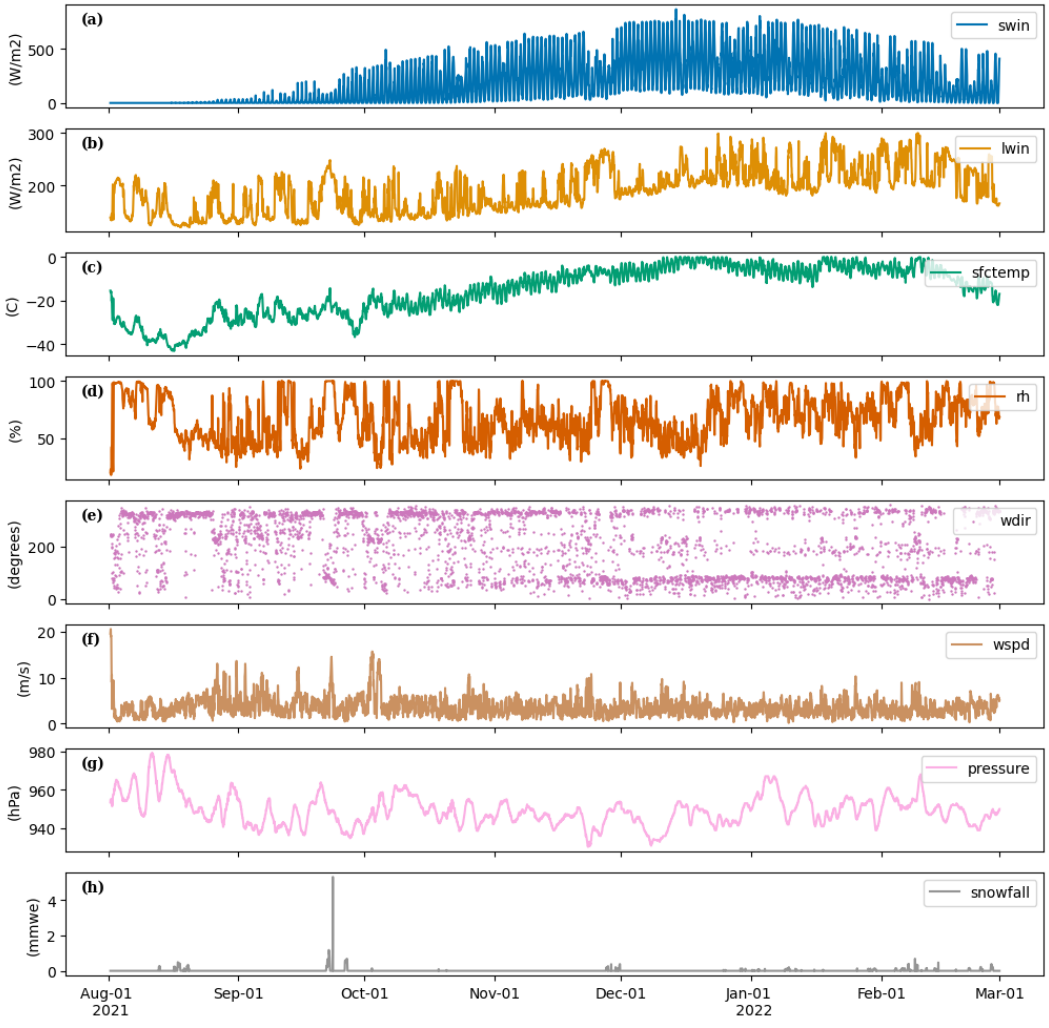

Figure 2. (a) Average hourly incoming shortwave radiation, incoming longwave radiation, surface temperature, relative humidity, wind direction, wind speed, pressure and snowfall measured at COHM AWS (1 August to 30 November 2021) and CWG AWS (1 December 2021 to 28 February 2022). Pressure is from the Antarctic Mesoscale WRF Prediction System (AMPS) for the first period as it was not measured at COHM AWS.

3.4 Implementation and initialization

In this model experiment, the standalone version of WRF-Hydro/Glacier V5.2.0 was used to limit uncertainties in meteorological forcing data introduced when coupled to WRF. Here a horizontal grid spacing of 200 meters at an hourly time step was used for the land surface and snowpack models, although only the grid cell on Commonwealth Glacier is analyzed to test the model with observed meteorology as input. Crocus was initialized with 40 layers (as in Eidhammer et al. (2021)) and constant

https://doi.org/10.5194/egusphere-2023-835
Preprint. Discussion started: 24 May 2023

thickness of 50 meters for simplicity and in line with observations of terminal cliff heights. The glacier temperatures were initialized at -18 °C for each layer and with a constant temperature of -18 °C at the soil-glacier boundary since the temperature at this depth is expected to be the annual mean air temperature.

The model spin-up period was 1 August to 30 November 2021 to obtain a realistic ice temperature profile at the start of the simulation. Ice temperatures at the end of the spin-up period were analyzed to ensure that the spin-up time was sufficient. Following the spin-up period, the different model configurations were validated from 1 December 2021 to 28 February 2022. This period was chosen because there is no observed runoff outside of these months. Ice surface temperatures reach the melting point for the first time in December and the temperatures drop below the melting point in February. More information on the model configuration can be found in the namelists provided in *Code and data availability*.

3.5 Validation Data

The model is validated using surface temperature, internal ice temperatures, albedo, surface height change and streamflow over the melt season. Ice surface temperature was calculated from outgoing longwave radiation (Table 1) using the Stefan-Boltzmann law and an emissivity of 1. Ice temperatures were obtained from thermocouples deployed at six different depths (Table 1). A two week validation period in early December was chosen as the top two thermocouple sensors melted out after the first two weeks of December. Observed albedo was calculated as accumulated albedo, by taking a moving mean over 24 hours for the ratio of accumulated outgoing shortwave radiation (absolute value) over accumulated incoming shortwave radiation (Van Den Broeke et al., 2004). This method is used in polar regions to limit uncertainty associated with changing solar zenith angle with the midnight sun. As noted in Section 3.3, surface height change was obtained using the K nearest neighbors regression used for pre-processing precipitation to eliminate noise from the sensor. Finally, streamflow data came from the Lost Seal stream gauge (Doran and Fountain, 2022) and were used to validate the temporal variation in simulated runoff.

4 Modifications

This section describes the two different schemes in Crocus that required modification: vertical percolation of water through the snowpack and spectral albedo. First, we describe the processes accounted for in the model and the challenges these schemes pose for a cold-based MDV glacier. This is followed by a description of the modifications made.

4.1 Water drainage through snowpack/glacier

Eidhammer et al. (2021) implemented WRF-Hydro/Glacier on a temperate glacier in Norway with internal temperatures initialized at 0 °C. Runoff in the summer is generated by precipitation (rain) in addition to melt. In contrast, the MDV glaciers are cold-based with internal temperatures around -18 °C and runoff is entirely from surface and near-surface glacial melt. Due to the extreme differences in these two environments, modifications to the snowpack/ice water flow and spectral albedo schemes

https://doi.org/10.5194/egusphere-2023-835
Preprint. Discussion started: 24 May 2023

were necessary in order to adapt Crocus embedded in WRF-Hydro to this environment.

As a snowpack model, runoff in the original WRF-Hydro/Glacier is calculated as the remaining water after it has percolated through all of the layers and reached the ice-soil interface. In this version of the model, ice is not treated differently to snow layers and the ice remains porous. This is problematic because it allows the meltwater to percolate through the ice layers rather than having the ice layers act as a barrier (MacDonell, 2008; Bergstrom et al., 2021). As the water percolates through, it can refreeze in a layer depending on temperature and energy or it can be held in the layer as liquid water content. The left panel of Fig. 3 depicts the water flow scheme from WRF-Hydro/Glacier (oldrunoff) for a single hour in the top 40 cm or 4 layers of the glacier. The oldrunoff plot shows that meltwater is generated in Layer 1 and a portion of that melt is held in the layer as liquid water content since it is a snow layer. The remaining meltwater percolates down to Layer 2. This is an ice layer. Some of the percolated water refreezes and a smaller amount is held as liquid water content of the layer. Any remaining water continues to percolate to the layer below, Layer 3, where all of it refreezes and thus, there is no runoff. Runoff is only possible in oldrunoff if the entire glacier is at the melting point such that the liquid water can percolate through the entire glacier or snowpack column. This does not align with MDV observations of near-surface melt with subfreezing subsurface (Hoffman et al., 2014). Thus, we introduce a condition such that if the liquid water reaches an ice layer, a portion refreezes and all remaining water becomes runoff. This allows the ice to be a barrier and results in the generation of near-surface runoff. The effect of this modification can be seen in the right panel of Fig. 3, newrunoff. Here, the top snow layer is similar to the oldrunoff panel and a portion of the water that percolates through the top snow layer refreezes on Layer 2. The difference is that there is no liquid water held in Layer 2, since the ice layers are no longer porous and have a liquid water holding capacity of zero. The remaining liquid water from Layer 2 becomes runoff since the ice layer is a barrier preventing further percolation. Thus, there is 0.11 mm of runoff.

4.2 Crocus Spectral Albedo Scheme

Energy for melt on MDV glaciers comes from solar radiation and albedo is an important factor in controlling this energy (Macdonell et al., 2013; Bergstrom et al., 2020). The spectral albedo scheme was not suitable for modelling the evolution of albedo on an MDV glacier as the snow albedo scheme was optimized for Col de Porte in France (Brun et al., 1992) and the ice albedo scheme for two glaciers in the French Alps (Gerbaux et al., 2005).

In this section, we describe how broadband albedo is calculated from spectral albedo in WRF-Hydro/Glacier, provide the rationale for modifying the parameters in the albedo scheme and the new parameters tuned to observations of spectral albedo.

4.2.1 Description of albedo scheme

The Crocus albedo scheme implemented in WRF-Hydro/Glacier is currently calculated over three spectral bands, where Band 1 is the visible band with wavelengths from 0.3-0.8 μm, Band 2 is the red band with wavelengths from 0.8-1.5 μm and Band 3 is the near infra-red band with wavelengths from 1.5-2.8 μm. The albedo in each band is calculated for the top two layers of

https://doi.org/10.5194/egusphere-2023-835
Preprint. Discussion started: 24 May 2023

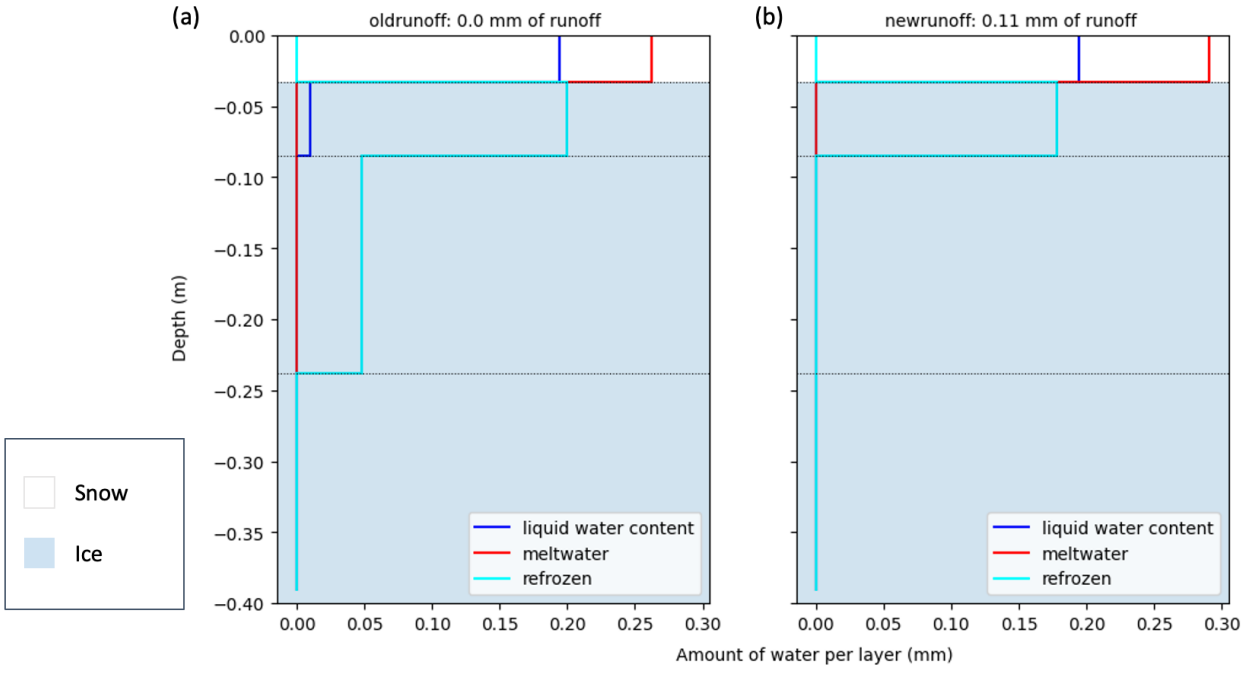

Figure 3. A comparison between the (a) original runoff scheme from Crocus (oldrunoff) and the (b) new modified runoff scheme (newrunoff). Cross sections show the top 40 cm and the total amount of liquid water held in the layer (blue), the total amount of water melted (red) and total amount refrozen (cyan) for each layer at 3:00 UTC 10 December 2021. The white and blue background colors show which layers are snow and ice respectively. Horizontal black dotted lines denote the different layers.

the snowpack or glacier using different schemes for ice and snow.

The snow albedo scheme in WRF-Hydro/Glacier is based on the theoretical studies of Warren (1982). Albedo for each band ($i = 1..3$) of the two top layers ($j = 1, 2$) is calculated in the following equations:

$$\begin{cases} \alpha_1^j & = \max(S_{1a}, \min(S_{1b}, S_{1c} - S_{1d}\sqrt{d_{\text{opt}}^j}) - \min(1, \max(\frac{P}{870}, 1.5)) \times 0.2\frac{A^j}{60}) \\ \alpha_2^j & = \max(S_{2a}, S_{2b} - S_{2c}\sqrt{d_{\text{opt}}^j}) \\ \alpha_3^j & = S_{3a}d'^j - S_{3b}\sqrt{d'^j} + S_{3c}, \end{cases} \tag{1}$$

where S are various snow model parameters (see Table 2). d_{opt} is the optical diameter of the snow grains, P is the mean surface pressure in hectopascals, A is the snow age in days and d' is $\min(d^{opt}, 0.0023)$ for each layer, j. All of the constants in the three equations correspond to parameters (see columns 1 and 2 in Table 2) that can be altered in the Crocus namelist.

https://doi.org/10.5194/egusphere-2023-835
Preprint. Discussion started: 24 May 2023

For ice layers (density > 850 kg m$^-3$), the albedo of the three bands ($\alpha_1, \alpha_2, \alpha_3$) is:

$$\alpha_i^j = I_i, \quad i = 1..3, j = 1, 2 \tag{2}$$

where I_i are the constant values for ice for the three bands (i) listed in Table 2.

Next, a weight (f) is calculated for both layers as a function of the thickness of each layer and various parameters:

$$f^1 = 0.8 \times \min(1, \frac{\Delta z^1}{0.02}) + 0.2 \times \min(1, \max(0, \frac{\Delta z^1 - 0.02}{0.01})) \tag{3}$$

$$f^2 = 0.8(1 - \min(1, \frac{\Delta z^1}{0.02})) + 0.2(1 - \min(1, \max(0, \frac{\Delta z^1 - 0.02}{0.01}))), \tag{4}$$

where Δz^1 is the thickness of the first layer.
The total albedo of each band (α_i), is then

$$\alpha_i = f^1 \alpha_i^1 + f^2 \alpha_i^2, \quad i = 1..3. \tag{5}$$

The broadband albedo is a weighted average of the total albedo of each band:

$$\alpha = 0.71\alpha_1 + 0.21\alpha_2 + 0.08\alpha_3. \tag{6}$$

4.2.2 Motivation for tuning the parameters

Fig. 4 shows the observed broadband albedo from 1 December to 28 February. There was snowfall at the end of November (Fig. 2h) so on 1 December the timeseries begins with snow that is no longer fresh. The surface has a broadband albedo of 0.7, then the surface transitions from snow to ice on 20 December with an albedo of 0.55. After, there are a few snowfall events (e.g. 24, 26, 30 December and 5, 11 January) that increase albedo and decrease slowly after each snowfall. Looking at modelled albedo, the oldalbedo (Fig. 4) begins with a snow albedo of 0.81 then the surface transitions to ice with a constant albedo of 0.2 on 13 December. Each time it snows, the albedo increases briefly, then rapidly decays to ice.

The issues are 1) the modelled ice albedo is too low compared to the observations (0.2 vs. 0.55) and 2) the modelled snow albedo does not match the observations (0.7 vs 0.81). The ice albedo in observations reaches only down to 0.48 and is similar to the range of minimum albedo measured by Bergstrom et al. (2020) of approximately 0.4-0.5 on Commonwealth Glacier over three melt seasons. Hoffman (2011) similarly found a minimum of $\sim$0.53. These values are higher than temperate glaciers because of minimal sediment and impurities on the glacier and low amounts of meltwater (that has not drained) that can lower albedo (Hoffman, 2011). The snow albedo observations at the beginning of the period is lower than the modelled snow albedo. Observed snow albedo over the melt season is also similar to the albedo observations from Bergstrom et al. (2020), however the values for fresh snow are often lower than those observed in other glaciated locations. For example, Reijmer et al. (2001) recorded an average snow albedo of 0.78 at a point in Dronning Maudland, Antarctica, whilst the average snow albedo in this

https://doi.org/10.5194/egusphere-2023-835
Preprint. Discussion started: 24 May 2023

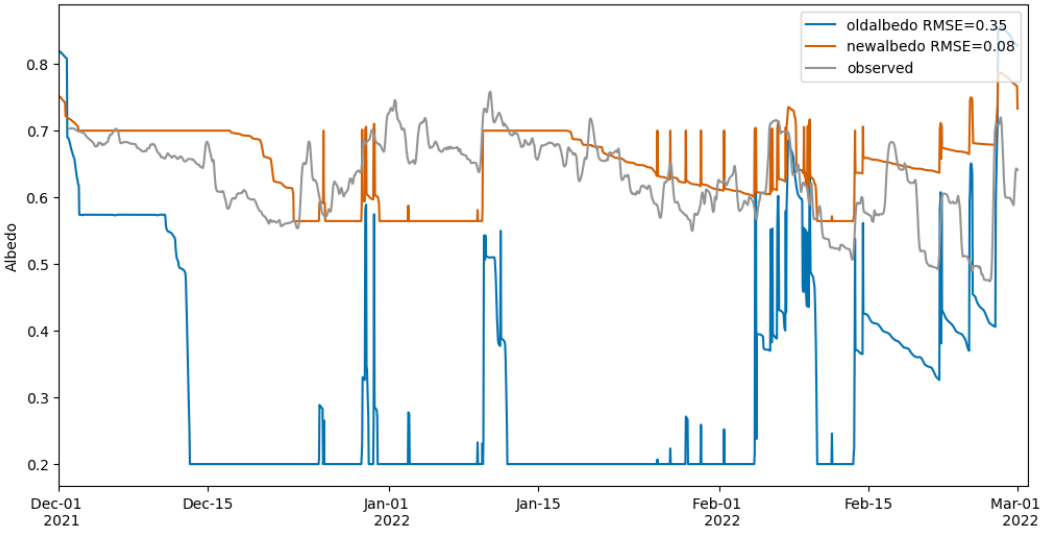

Figure 4. Comparison between the broadband albedo of the original Crocus scheme in blue, the modified scheme in orange and the observed daily accumulated albedo in grey.

study is ∼0.65. This is likely because there are very little snowfall amounts in the MDV and the albedo will be a combination of thin surface snow and the lower albedo ice beneath. The parameters in the model snow albedo scheme are based on modelled snow albedo in Warren (1982) and the parameters are optimized for the French Alps (Brun et al., 1992). The ice albedo scheme is constant and has been tuned to glaciers in the French Alps (Gerbaux et al., 2005). Thus, the parameters of the model albedo scheme must be modified to the MDV environment.

4.2.3 Modifying the albedo scheme parameters

This subsection describes the method by which new parameters were chosen for the spectral albedo scheme. We chose to tune the albedo scheme for December 2021 and test the new parameters from 1 January to 28 February 2022. In this study, we opted to use observed spectral albedo profiles measured by Dadic et al. (2013) in Allan Hills, East Antarctica as they provide similar information to Warren (1982), but for a location that is closer to our field site on Commonwealth Glacier.

First, we determine new parameters for the ice albedo bands by calculating the average spectral albedo of each band from Dadic et al. (2013, Fig. 6) for the different types of ice (white and blue ice). These values were then tuned to the minimum observed broadband albedo during December 2021, whilst ensuring that the value of each band remained in the range of average values from Dadic et al. (2013, Fig. 6). The effect of this tuning process for ice albedo is shown in the period 13-25 December in Fig.

https://doi.org/10.5194/egusphere-2023-835
Preprint. Discussion started: 24 May 2023

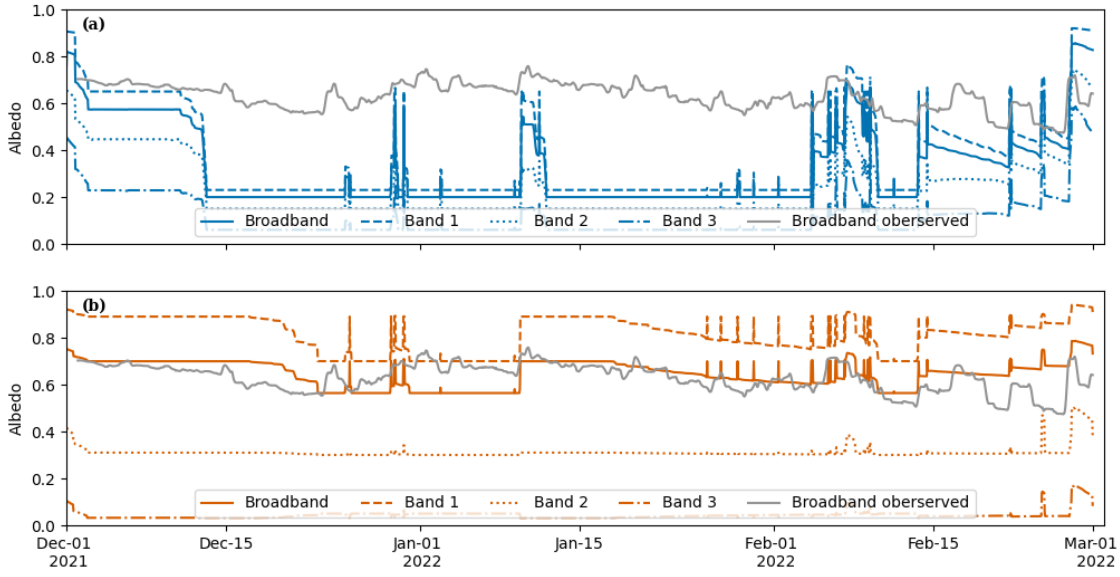

Figure 5. Comparison between the daily accumulated broadband albedo in grey and three spectral albedo bands of (a) the original Crocus albedo in blue and (b) the modified scheme in orange.

4, where the newalbedo scheme is much closer to the broadband albedo observed on the ice surface in this period.

Next, we modified the maximum and minimum spectral albedo in each band based on observations by Dadic et al. (2013) (Band 1 are S_{1b} and S_{1a}, respectively and Band 2, S_{2b} and S_{2a}). Band 3 is slightly more complex. Here, we solved a system of equations using the largest and smallest optical diameters from the oldalbedo model run to represent snow and firn over the tuning period. These maxima and minima were constrained by averages calculated from Fig. 6 in Dadic et al. (2013) for snow and firn and tuned to observed broadband albedo (S_{3b} and S_{3c}). The new parameter choices are in bold in Table 2. Fig. 5a shows the effect of the new parameters on the three bands and the broadband albedo over the full melt season in the “newalbedo" model run. The newalbedo scheme has bands that are separate and are aligned with the theory as well as observations in Dadic et al. (2013)’s study. The root mean square error (Fig. 4) is improved by 0.27 in the newalbedo model compared to the oldalbedo model. The newalbedo model captures the variability in albedo, without overfitting to the observations.

https://doi.org/10.5194/egusphere-2023-835
Preprint. Discussion started: 24 May 2023

Table 2. Parameters from original Crocus compared to the new scheme. Bold indicates changed parameters. We introduce a new parameter, XVALB12 (S_{2a}) to specify the minimum albedo for Band 2 as the original value was hard coded.

Snow albedo				
	Parameter	oldalbedo	newalbedo	Name in code
Band 1	S_{1a}	0.65	**0.89**	XVALB11
	S_{1b}	0.92	**0.94**	XVALB4
	S_{1c}	0.96	0.96	XVALB2
Band 2	S_{2a}	0.3	**0.31**	XVALB12 (new parameter)
	S_{2b}	0.9	**0.66**	XVALB5
	S_{2c}	15.4	15.4	XVALB6
Band 3	S_{3a}	346.3	346.3	XVALB7
	S_{3b}	32.31	**21.0**	XVALB8
	S_{3c}	0.88	**0.35**	XVALB9
Ice albedo				
Band 1	I_1	0.23	**0.7**	XALBICE1
Band 2	I_2	0.15	**0.3**	XALBICE2
Band 3	I_3	0.06	**0.05**	XALBICE3

5 Model comparison and evaluation

In this section, we evaluate three different versions of the model code representing the original scheme (oldrunoff_oldalbedo), updates to both runoff and albedo schemes (newrunoff_newalbedo) and updates only to the runoff scheme (newrunoff_oldalbedo). The versions are evaluated against observations of surface temperature, ice temperatures and surface height change over summer 2021/22. Finally, the differences in simulated runoff between the three models is presented and discussed.

5.1 Surface temperature

Fig. 6 shows the performance of the different models compared to the observed surface temperatures at the AWS over the second half of December. The timeseries shows that the newrunoff_newalbedo daytime surface temperature drops below the melting point from 26-30 December similarly to observed surface temperatures, while the two previous versions of the model (oldrunoff_oldalbedo and newrunoff_oldalbedo) reach the melting point daily for the period. This is more evident in Fig. 7, the two models using the original albedo scheme have similar root mean square errors (Fig. 7a, b), however the root mean square error of the newrunoff_newalbedo (Fig. 7c) run is 60% less than newrunoff_oldalbedo and 62% less than oldrunoff_oldalbedo. Furthermore, the newrunoff_newalbedo model has a more equal spread on either side of the 1-1 line around the melting point

https://doi.org/10.5194/egusphere-2023-835
Preprint. Discussion started: 24 May 2023

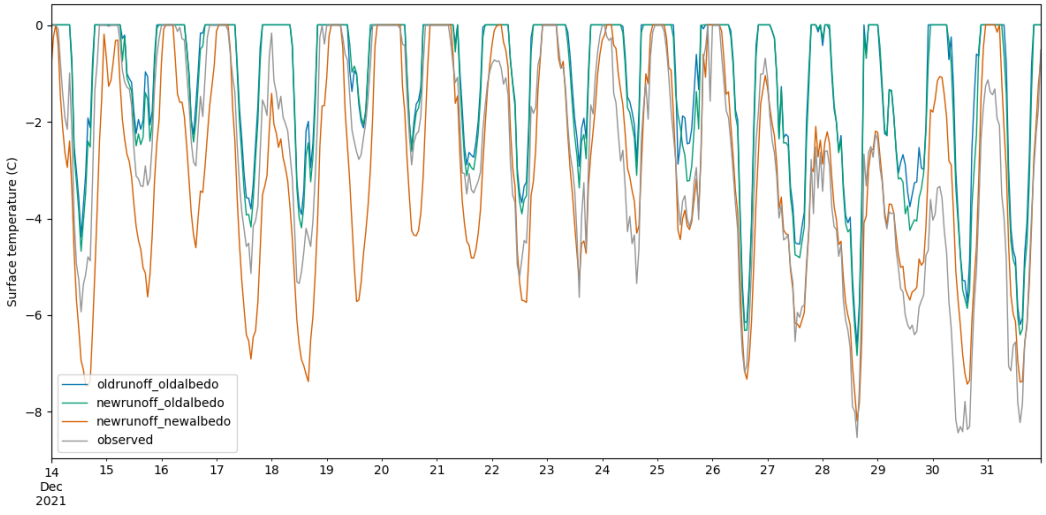

Figure 6. Comparison between the three different versions of the model and the observed surface temperatures over the last two weeks in December 2021.

compared to the two models with the original albedo scheme, which both overestimate the number of hours with surface temperature at the melting point as seen by the aggregation of points on the top left of the 1-1 line. The percent of time (hours) each model is at the melting point is 25.8 % (557.3 hours) for oldrunoff_oldalbedo, 24.5 % (529.2 hours) for newrunoff_oldalbedo and 5.7 % (123.12 hours) for newrunoff_newalbedo, compared to 5.0 % (108.0 hours) for observed surface temperatures. In comparison, Hoffman et al. (2014) found that on average there were 255.1 hours of surface and near-surface melt with a maximum of 452 and a minimum of 92 hours from 1996-2009 on Taylor Glacier. Thus the values for the newrunoff_newalbedo model are similar to the average, while oldrunoff_oldalbedo and newrunoff_oldalbedo are greater than the maximum number of hours found by Hoffman et al. (2014).

For temperatures around -20 °C, newrunoff_newalbedo has a slight cold bias which can also be seen in the daily minimums in Fig. 6. This is likely due to the observed albedo being lower than the modelled albedo during this period as seen in Fig. 4.

5.2 Internal ice temperatures

Internal ice temperatures at six different depths are validated for the three model runs in Table 3. This shows that newrunoff_newalbedo has the lowest root mean square errors for internal ice temperatures, especially for the near-surface layers TC1-4. Fig. 8 shows the temporal variability of the modelled vs observed ice temperatures for the newrunoff_newalbedo model. The modelled temperatures agree with the measured temperatures and are often within 1 °C of the measurement. The root mean square errors for TC2-6 all lie below one except for at TC1, which matches observations at the beginning of the period, but has a cold bias later

https://doi.org/10.5194/egusphere-2023-835
Preprint. Discussion started: 24 May 2023

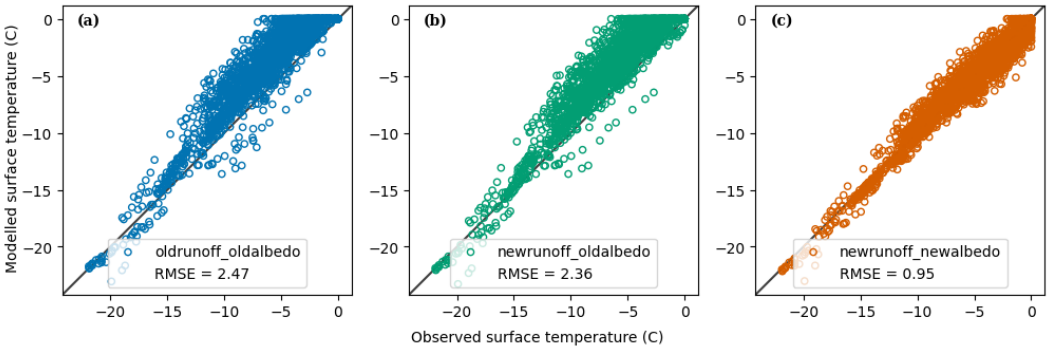

Figure 7. A scatter plot with modelled surface temperatures vs. observed surface temperatures for the three models from December 2021 through February 2022.

Table 3. Root mean square errors of the internal ice temperatures of the three model versions at six different depths from 1-15 December 2021.

	oldrunoff_oldalbedo	newrunoff_oldalbedo	newrunoff_newalbedo
TC1	2.36	2.27	1.58
TC2	2.26	1.91	0.9
TC3	2.63	1.96	0.53
TC4	2.24	0.7	0.56
TC5	1.25	0.66	0.88
TC6	0.28	0.28	0.27

in the period. The first time step of the validation period beginning 1 December shows that the model is in good agreement with the observations and gives us confidence that a longer spin-up is not necessary. The model also captures both the diurnal cycle as well as the seasonal warming seen in TC4, TC5 and TC6. This can also be seen in Fig. 9, which shows a cross section of ice temperatures in the top 3 meters of the glacier modelled by newrunoff_newalbedo from August 2021 through February 2022. Darker blues indicate the cooling of the glacier during the spin-up period (August-November 2021) and then the warming period beginning in December. However, there is a slight delay in the diurnal cycle of the measurements compared to the model in Fig. 8. This could be due to differences in the solar penetrating radiation that result in the glacier not warming enough compared to the measurements. Overall, the model does a satisfactory job of modelling the near-surface ice temperatures as seen in the root mean square errors in Fig. 8, which is important for generating near-surface melt.

https://doi.org/10.5194/egusphere-2023-835
Preprint. Discussion started: 24 May 2023

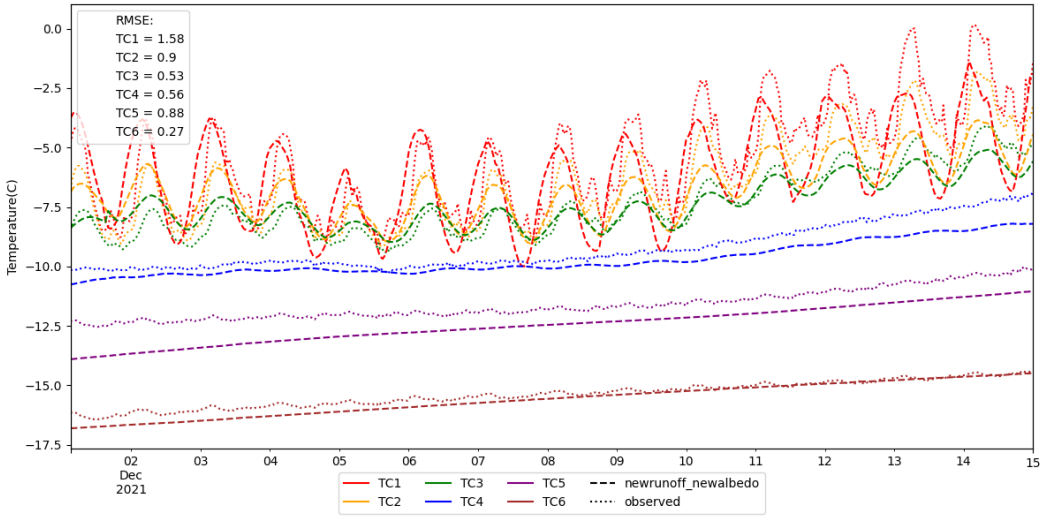

Figure 8. Modelled internal ice temperatures from newrunoff_newalbedo over the first two weeks of December. Thermocouples were initially deployed at six different depths: 0.05, 0.1, 0.2, 0.5, 1.0 and 2.0 meters. Note that the measurements are not at a constant depth with time as the sensors were melting out over the period. This shows diurnal variability at shallower depths and the seasonal warming wave below.

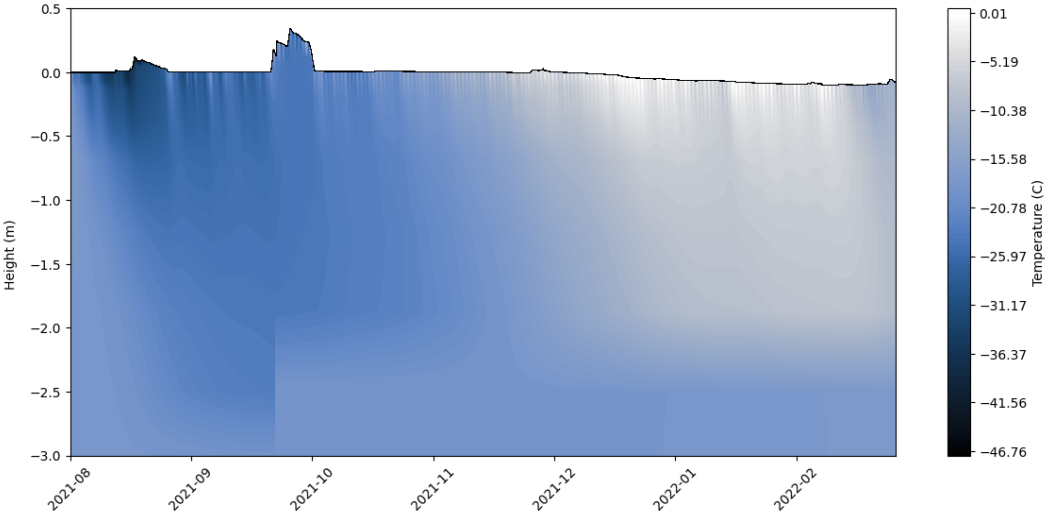

Figure 9. Cross section of modelled temperature from newrunoff_newalbedo of the top three meters of the glacier over the spin-up period of August-November and validation period of December-February. This shows the diurnal variability at shallower depths and the seasonal cooling then warming wave below.

https://doi.org/10.5194/egusphere-2023-835
Preprint. Discussion started: 24 May 2023

5.3 Surface height change

Fig. 10 shows the surface height from 1 December 2021 to 28 February 2022 of the three model versions compared with observations of surface height. Although the three models begin December in alignment (same spin-up), they begin to diverge a couple days later. The newrunoff_newalbedo scheme remains most similar to the observed surface height with a root mean square error of 0.02 (Fig. 10). The oldrunoff_oldalbedo scheme clearly performs the worst, losing around 35 cm more than the observations over the three month period and with a root mean square error of 0.26 (Fig. 10). The newrunoff_oldalbedo performance is similar to newrunoff_newalbedo, but with a root mean square error of 0.05 (Fig. 10). Thus, it is evident that optimizing the parameters for the albedo scheme and modifying the drainage through the glacier was needed to accurately simulate the surface height change.

The differences between the surface height change of the three models occur during the first three weeks of December. After 23 December, the three models have a similar change in surface height; oldrunoff_oldalbedo has 90 cm ablation, newrunoff_oldalbedo has 10 cm ablation and newrunoff_newalbedo has 3 cm ablation compared to 10 cm observed ablation. On 6 December, oldrunoff_oldalbedo and newrunoff_oldalbedo reach the melting point for the first time and the suface height lowers faster than newrunoff_newalbedo. On 13 December, the TC1-3 near-surface ice temperatures of oldrunoff_oldalbedo reach the melting point (Fig. A1), whilst newrunoff_oldalbedo near-surface ice temperatures remain below the melting point (Fig. A2). This rapid decrease in surface height and warming of the glacier layers for oldrunoff_oldalbedo may be due to near-surface melt that is percolating through ice layers and subsequently warming them, rather than draining as near-surface runoff as modified in newrunoff_oldalbedo. This can be seen in Fig. A1 for oldrunoff_oldalbedo, where TC1 reaches the melting point on 12 December then internal ice temperatures for TC2-5 increase rapidly from 13 December. On the other hand, in Fig. A2, TC1 from newrunoff_oldalbedo reaches the melting point on 13 December, but TC2-5 do not increase as much as in oldrunoff_oldalbedo.

5.4 Runoff

Although we do not have site specific runoff measurements for this location, stream gauge observations of the Lost Seal catchment on Commonwealth Glacier indicate that melt and runoff are activated episodically, rather than consistently melting daily over the melt season (Fig. 11c). Fig. 11a shows the daily accumulated runoff in millimeters of liquid water for the three different models. The oldrunoff_oldalbedo model has no runoff during the entire period of the melt season due to the percolation and subsequent refreezing of meltwater through the ice layers that was modified for the newrunoff models. On the other hand, the newrunoff_oldalbedo model has generated runoff almost daily throughout the season from 10 December with a daily maximum of 45.0 mm. The newrunoff_newalbedo model has more episodic runoff with a daily maximum of 5.1 mm.

Fig. 11a, b show the runoff is generated earlier and is larger in the newrunoff_oldalbedo model runoff than the newrunoff_newalbedo model. This is because the albedo falls to the ice albedo on the day that runoff is activated for the season (Fig. 4). On the other

https://doi.org/10.5194/egusphere-2023-835
Preprint. Discussion started: 24 May 2023

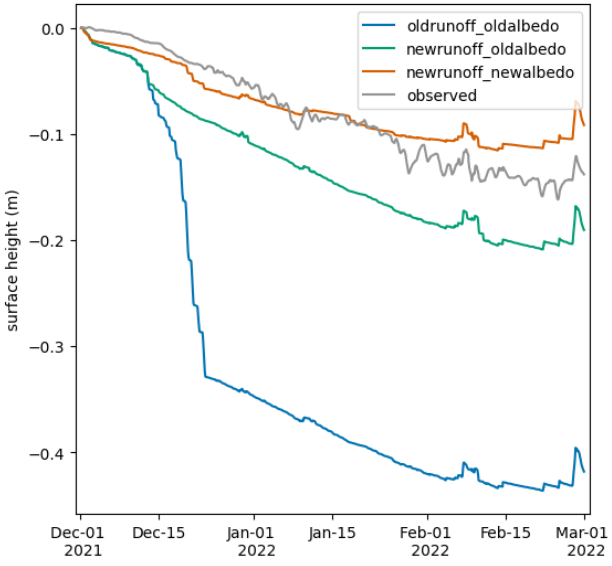

Figure 10. The change in surface height (m) between the three models and the quarter-hourly observational data.

hand, the newrunoff_newalbedo model runoff is more ephemeral compared to the newrunoff_oldalbedo model. When we compare the runoff with the surface temperatures from Fig. 6, it can be seen that runoff is activated when ice surface temperatures reach the melting point and the runoff shuts off when the temperature drops below the melting point.

Furthermore, we can compare the daily average modelled runoff from newrunoff_newalbedo to the daily average stream gauge observations (Doran and Fountain, 2022) in Fig. 11c. Although we cannot compare the magnitudes, this shows that we are accurately capturing the temporal variability and episodic nature of melt in the MDV (Fig. 11c). Modelled runoff is not accounting for the physical processes of water drainage off-glacier, such as evaporation or soil absorption and this may explain some of the differences between the stream gauge and model. Hoffman et al. (2014) calculated a range of 11.2 to 152.0 mm water-equivalent of total subsurface drainage and surface melt per melt season over 13 years at a point on Taylor Glacier. The total runoff over the melt season in our study was 858 mm water-equivalent for the newrunoff_oldalbedo run and 36 mm water-equivalent for the newrunoff_newalbedo run. The total runoff for the newrunoff_newalbedo run lies in the range from Hoffman et al. (2014). Thus, we are confident that the newrunoff_newalbedo run is modelling the frequency and magnitude runoff accurately.

5.5 Limitations

We implemented the WRF-Hydro/Glacier model at a point on Commonwealth Glacier and forced the model with observational data in order to limit the input uncertainties to the model that would be introduced if using a larger spatial resolution/gridded

https://doi.org/10.5194/egusphere-2023-835
Preprint. Discussion started: 24 May 2023

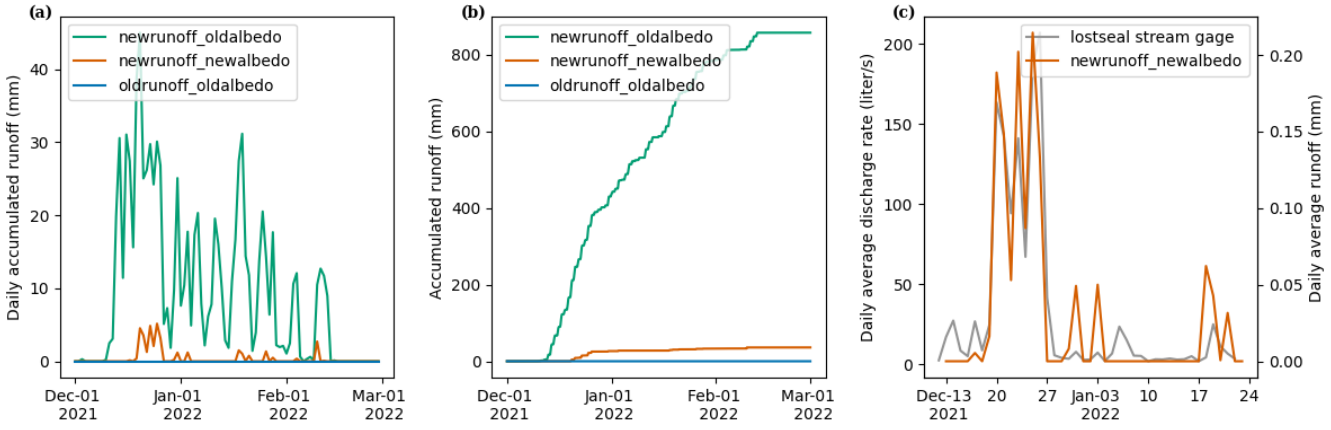

Figure 11. (a) Daily accumulated runoff and (b) cumulative runoff from the three model runs from 1 December 2021 - 28 February 2022. (c) Daily average discharge from the lost seal stream gauge (grey) compared to modelled daily average runoff (orange) from newrunoff_newalbedo.

atmospheric model data. However, there still exist a few uncertainties in the input data, especially regarding precipitation. Precipitation was calculated from the change in snow height record, but this was challenging as the data are noisy and summer snow accumulation is very small, but can have significant impacts on the albedo and on melt generation (Fountain et al., 2010). Temperature and wind speed can impact the sonic ranging sensor that measures the snow height and contribute to the noise in the data. The threshold for snow was tuned on a monthly basis and was smaller than both the instrument accuracy and the thresholds from Fountain et al. (2010) and Myers et al. (2022), which would have filtered out all of the summer snowfall events seen in observed albedo.

Other limitations to this study are the short time period used for spin-up, tuning and testing the model. We demonstrated that the four month spin-up was sufficient to accurately simulate the internal ice temperatures. Although a longer time period could be helpful for tuning and testing the model, this study was a proof of concept and the model demonstrated that one month of tuning was sufficient to simulate the evolution of the broadband albedo for January and February without overfitting.

6 Future Research and outlook

Implementing WRF-Hydro/Glacier forced by AWS data at a point is similar to previous studies that have implemented surface energy and mass balance models at a point on a MDV glacier (Hoffman et al., 2008; Macdonell et al., 2013; Hofsteenge et al., 2022). However this method allowed us to adjust the model in order to accurately simulate the processes of melt generation and shows that we are obtaining “the right answers for the right reasons" (Kirchner, 2006). Future research will be able to build

https://doi.org/10.5194/egusphere-2023-835
Preprint. Discussion started: 24 May 2023

on this by modelling the spatially distributed melt and hydrological connectivity in Taylor and Wright valleys. For example, Bergstrom et al. (2020) measured spatial albedo for a few helicopter swaths show that albedo increased on MDV glaciers with elevation and towards the west of the ablation area. Since albedo is one of the main drivers of melt, optimizing the spectral albedo parameters in this study to simulate the evolution of broadband albedo means that this model has the potential to simulate changes in the spatial distribution of albedo at the valley scale. This study is the first in the MDV to simulate albedo rather than using point observations of albedo to force a model (Hoffman, 2011; Hofsteenge et al., 2022). In turn, this modelling framework can answer questions regarding the impact of such spatial albedo gradients on the hydrological system. In addition, the modified WRF-Hydro/Glacier model will also allow us to expand on the work from Hoffman (2011) and Cross et al. (2022) by accounting for in-stream processes such as evaporation and absorption of meltwater in the soil. These have a greater impact on the streamflow amounts in low melt years. Furthermore, explicitly modelling the stream channels will allow us to answer questions around the timing between melt generation and lake inflow, which has downstream impacts on the nutrient availability for the microbial ecosystem (Gooseff et al., 2017; Singley et al., 2021). Finally, this model can also be used to test the hydrological response to atmospheric warming with climate sensitivity tests. In the end, such modelling efforts help us to understand how the MDV ecosystem dependent on meltwater and streams may change in response to future climate.

WRF-Hydro/Glacier is a model that can be applied at different scales and environments. Here, we have tested the use of WRF-Hydro/Glacier in an extreme MDV polar environment. We found it was necessary to modify two schemes to reliably simulate the surface energy balance and runoff of a cold-based MDV glacier:

- Preventing the percolation of meltwater through ice layers to allow near-surface runoff and
- Tuning the spectral albedo parameters for both snow and ice based on observed spectral signatures to model the evolution of broadband albedo and net shortwave radiation.

With these modifications, we were able to accurately simulate the broadband albedo, near-surface ice temperatures, surface height change and produce realistic runoff over a melt season. The next step is to scale the current model to the valley scale to better understand runoff dynamics over different glacial catchments in the MDV.

Code and data availability. Code of the modified WRF-Hydro/Glacier for a cold-based glacier is available on github (https://github.com/tpletzer/wrf_hydro_nwm_coldglacier).

Author contributions. TP, JPC, NJC and MK designed the study. TP and JPC devised the methodology. TP implemented and modified WRF-Hydro/Glacier, collected CWG AWS data and produced the results. TE provided expert advice on the WRF-Hydro/Glacier model. TP, JPC and NJC contributed to the analysis. TP wrote the manuscript with edits from the co-authors. MK provided funding for the field work.

https://doi.org/10.5194/egusphere-2023-835
Preprint. Discussion started: 24 May 2023

Competing interests. The contact author has declared that they do not have any competing interests.

Disclaimer. Publisher's note: Copernicus Publications remains neutral with regard to jurisdictional claims in published maps and institutional affiliations.

Acknowledgements. This research has been supported by the Antarctic Science Platform (grant no. ANTA1801) and the Royal Society of New Zealand (grant no. RDF-UOC1701). We would also like to thank University of Otago for funding this research. The authors wish to acknowledge the use of New Zealand eScience Infrastructure (NeSI) high performance computing facilities and consulting support as part of this research. New Zealand's national facilities are provided by NeSI and funded jointly by NeSI's collaborator institutions and through the Ministry of Business, Innovation and Employment's Research Infrastructure programme https://www.nesi.org.nz.

https://doi.org/10.5194/egusphere-2023-835
Preprint. Discussion started: 24 May 2023

References

Bergstrom, A., Gooseff, M. N., Myers, M., Doran, P. T., and Cross, J. M.: The seasonal evolution of albedo across glaciers and the surrounding landscape of Taylor Valley, Antarctica, Cryosphere, 14, 769–788, https://doi.org/10.5194/tc-14-769-2020, 2020.

Bergstrom, A., Gooseff, M., Fountain, A., and Hoffman, M.: Long-term shifts in feedbacks among glacier surface change, melt generation and runoff, McMurdo Dry Valleys, Antarctica, Hydrological Processes, 35, https://doi.org/10.1002/hyp.14292, 2021.

Brandt, R. E. and Warren, S. G.: Solar-heating rates and temperature profiles in Antarctic snow and ice, Journal of Glaciology, 39, https://www.cambridge.org/core., 1993.

Brun, E., David, P., Sudul, M., and Brunot, G.: A numerical model to simulate snow-cover stratigraphy for operational avalanche forecasting, Journal of Glaciology, 38, 13–22, https://doi.org/10.3189/s0022143000009552, 1992.

Cross, J. M., Fountain, A. G., Hoffman, M. J., and Obryk, M. K.: Physical Controls on the Hydrology of Perennially Ice-Covered Lakes, Taylor Valley, Antarctica (1996–2013), Journal of Geophysical Research: Earth Surface, 127, https://doi.org/10.1029/2022JF006833, 2022.

Dadic, R., Mullen, P. C., Schneebeli, M., Brandt, R. E., and Warren, S. G.: Effects of bubbles, cracks, and volcanic tephra on the spectral albedo of bare ice near the Transantarctic Mountains: Implications for sea glaciers on Snowball Earth, Journal of Geophysical Research: Earth Surface, 118, 1658–1676, https://doi.org/10.1002/jgrf.20098, 2013.

Doran, P. and Fountain, A.: High frequency measurements from Commonwealth Glacier Meteorological Station (COHM), McMurdo Dry Valleys, Antarctica (1993-2021, ongoing), https://doi.org/10.6073/pasta/1fd2035c9efea9f105ecb1d6212448cc, 2022.

Eidhammer, T., Booth, A., Decker, S., Li, L., Barlage, M., Gochis, D., Rasmussen, R., Melvold, K., Nesje, A., and Sobolowski, S.: Mass balance and hydrological modeling of the Hardangerjøkulen ice cap in south-central Norway, Hydrology and Earth System Sciences, 25, 4275–4297, https://doi.org/10.5194/hess-25-4275-2021, 2021.

Fitzsimons, S. J.: Formation of thrust-block moraines at the margins of dry-based glaciers, south Victoria Land, Antarctica, Annals of Glaciology, 22, 68–74, https://doi.org/10.3189/1996aog22-1-68-74, 1996.

Fountain, A. G. and Doran, P. T.: Climatology of katabatic winds in the McMurdo dry valleys, southern Victoria Land, Antarctica, J. Geophys. Res, 109, 3114, https://doi.org/10.1029/2003JD003937, 2004.

Fountain, A. G., Nylen, T. H., Monaghan, A., Basagic, H. J., and Bromwich, D.: Snow in the Mcmurdo Dry Valleys, Antarctica, International Journal of Climatology, 30, 633–642, https://doi.org/10.1002/joc.1933, 2010.

Fountain, A. G., Basagic, H. J., and Niebuhr, S.: Glaciers in equilibrium, McMurdo Dry Valleys, Antarctica, Journal of Glaciology, 62, 976–989, https://doi.org/10.1017/jog.2016.86, 2016.

Gerbaux, M., Genthon, C., Etchevers, P., Vincent, C., and Dedieu, J. P.: Surface mass balance of glaciers in the French Alps: Distributed modeling and sensitivity to climate change, Journal of Glaciology, 51, 561–572, https://doi.org/10.3189/172756505781829133, 2005.

Gillett, S. and Cullen, N. J.: Atmospheric controls on summer ablation over Brewster Glacier, New Zealand, International Journal of Climatology, 31, 2033–2048, https://doi.org/10.1002/JOC.2216, 2011.

Gochis, D. J., Barlage, M., Cabell, R., Casali, M., Dugger, A., Fitzgerald, K., Mcallister, M., Mccreight, J., Rafieeinasab, A., Read, L., Sampson, K., Yates, D., and Zhang, Y.: The NCAR WRF-Hydro® Modeling System Technical Description v5.1.1, Tech. rep., NCAR, https://ral.ucar.edu/sites/default/files/public/WRFHydroV511TechnicalDescription.pdf., 2020.

Gooseff, M. N., McKnight, D. M., Doran, P., Fountain, A. G., and Lyons, W. B.: Hydrological connectivity of the landscape of the McMurdo Dry Valleys, Antarctica, Geography Compass, 5, 666–681, https://doi.org/10.1111/j.1749-8198.2011.00445.x, 2011.

https://doi.org/10.5194/egusphere-2023-835
Preprint. Discussion started: 24 May 2023

Gooseff, M. N., Wlostowski, A., McKnight, D. M., and Jaros, C.: Hydrologic connectivity and implications for ecosystem processes - Lessons from naked watersheds, Geomorphology, 277, 63–71, https://doi.org/10.1016/j.geomorph.2016.04.024, 2017.

Gooseff, M. N., McKnight, D. M., Doran, P. T., and Fountain, A.: Long-term stream hydrology and meteorology of a Polar Desert, the McMurdo Dry Valleys, Antarctica, Hydrological Processes, 36, https://doi.org/10.1002/hyp.14623, 2022.

Hoffman, M.: Spatial and Temporal Variability of Glacier Melt in Spatial and Temporal Variability of Glacier Melt in the McMurdo Dry Valleys, Antarctica the McMurdo Dry Valleys, Antarctica, Ph.D. thesis, Portland State University, Portland, https://doi.org/10.15760/etd.744, 2011.

Hoffman, M. J., Fountain, A. G., and Liston, G. E.: Surface energy balance and melt thresholds over 11 years at Taylor Glacier, Antarctica, Journal of Geophysical Research: Earth Surface, 113, https://doi.org/10.1029/2008JF001029, 2008.

Hoffman, M. J., Fountain, A. G., and Liston, G. E.: Near-surface internal melting: A substantial mass loss on Antarctic Dry Valley glaciers, Journal of Glaciology, 60, 361–374, https://doi.org/10.3189/2014JoG13J095, 2014.

Hofsteenge, M. G., Cullen, N. J., Reijmer, C. H., Van Den Broeke, M., Katurji, M., and Orwin, J. F.: The surface energy balance during foehn events at Joyce Glacier, McMurdo Dry Valleys, Antarctica, The Cryosphere, https://doi.org/10.5194/tc-2022-102, 2022.

Kerandi, N., Arnault, J., Laux, P., Wagner, S., Kitheka, J., and Kunstmann, H.: Joint atmospheric-terrestrial water balances for East Africa: a WRF-Hydro case study for the upper Tana River basin, Theoretical and Applied Climatology, 131, 1337–1355, https://doi.org/10.1007/s00704-017-2050-8, 2018.

Kirchner, J. W.: Getting the right answers for the right reasons: Linking measurements, analyses, and models to advance the science of hydrology, Water Resources Research, 42, https://doi.org/10.1029/2005WR004362, 2006.

Lahmers, T., Kumar, S., Dugger, A., Gochis, D., and Santanello, J.: Impacts of wildfires on the 2020 floods in southeast Australia: A vegetation data-assimilation case study using the NASA coupled LIS/WRF-Hydro system, https://doi.org/https://doi.org/10.5194/egusphere-egu21-9006, 2021.

Li, L., Gochis, D. J., Sobolowski, S., and Mesquita, M. D.: Evaluating the present annual water budget of a Himalayan headwater river basin using a high-resolution atmosphere-hydrology model, Journal of Geophysical Research, 122, 4786–4807, https://doi.org/10.1002/2016JD026279, 2017.

MacDonell, S.: Meltwater generation and drainage system on an Antarctic cold-based glacier, Ph.D. thesis, University of Otago, Dunedin, 2008.

Macdonell, S. A., Fitzsimons, S. J., and Mölg, T.: Seasonal sediment fluxes forcing supraglacial melting on the Wright Lower Glacier, McMurdo Dry Valleys, Antarctica, Hydrological Processes, 27, 3192–3207, https://doi.org/10.1002/hyp.9444, 2013.

Myers, M. E., Doran, P. T., and Myers, K. F.: Valley-floor snowfall in Taylor Valley, Antarctica, from 1995 to 2017: Spring, summer and autumn, Antarctic Science, 34, 325–335, https://doi.org/10.1017/S0954102022000256, 2022.

Nylen, T. H., Fountain, A. G., and Doran, P. T.: Climatology of katabatic winds in the McMurdo dry valleys, southern Victoria Land, Antarctica, Journal of Geophysical Research: Atmospheres, 109, https://doi.org/10.1029/2003JD003937, 2004.

Obryk, M. K., Doran, P. T., Fountain, A. G., Myers, M., and McKay, C. P.: Climate From the McMurdo Dry Valleys, Antarctica, 1986–2017: Surface Air Temperature Trends and Redefined Summer Season, Journal of Geophysical Research: Atmospheres, 125, https://doi.org/10.1029/2019JD032180, 2020.

Pal, S., Dominguez, F., Dillon, M. E., Alvarez, J., Garcia, C. M., Nesbitt, S. W., and Gochis, D.: Hydrometeorological Observations and Modeling of an Extreme Rainfall Event Using WRF and WRF-Hydro during the RELAMPAGO Field Campaign in Argentina, Journal of Hydrometeorology, https://doi.org/10.1175/JHM-D-20, 2021.

https://doi.org/10.5194/egusphere-2023-835
Preprint. Discussion started: 24 May 2023

Reijmer, C. H., Bintanja, R., and Greuell, W.: Surface albedo measurements over snow and blue ice in thematic mapper bands 2 and 4 in Dronning Maud Land, Antarctica, Journal of Geophysical Research Atmospheres, 106, 9661–9672, https://doi.org/10.1029/2000JD900718, 2001.

Senatore, A., Mendicino, G., Gochis, D. J., Yu, W., Yates, D. N., and Kunstmann, H.: Fully coupled atmosphere-hydrology simulations for the central Mediterranean: Impact of enhanced hydrological parameterization for short and long time scales, Journal of Advances in Modeling Earth Systems, 7, 1693–1715, https://doi.org/10.1002/2015MS000510, 2015.

Singley, J. G., Gooseff, M. N., McKnight, D. M., and Hinckley, E. S.: The Role of Hyporheic Connectivity in Determining Nitrogen Availability: Insights From an Intermittent Antarctic Stream, Journal of Geophysical Research: Biogeosciences, 126, https://doi.org/10.1029/2021JG006309, 2021.

Speirs, J. C., Steinhoff, D. F., McGowan, H. A., Bromwich, D. H., and Monaghan, A. J.: Foehn winds in the McMurdo Dry Valleys, Antarctica: The origin of extreme warming events, Journal of Climate, 23, 3577–3598, https://doi.org/10.1175/2010JCLI3382.1, 2010.

Steinhoff, D. F., Bromwich, D. H., and Monaghan, A.: Dynamics of the foehn mechanism in the Mcmurdo Dry Valleys of Antarctica from polar WRF, Quarterly Journal of the Royal Meteorological Society, 139, 1615–1631, https://doi.org/10.1002/qj.2038, 2013.

Van Den Broeke, M., Van As, D., and Reijmer, C.: Assessing and Improving the Quality of Unattended Radiation Observations in Antarctica, Journal of Atmopsheric and Oceanic Technology, 21, 1417–1431, 2004.

Vionnet, V., Brun, E., Morin, S., Boone, A., Faroux, S., Le Moigne, P., Martin, E., and Willemet, J. M.: The detailed snowpack scheme Crocus and its implementation in SURFEX v7.2, Geoscientific Model Development, 5, 773–791, https://doi.org/10.5194/gmd-5-773-2012, 2012.

Warren, S. G.: Optical properties of snow, https://doi.org/10.1029/RG020i001p00067, 1982.

Xiang, T., Vivoni, E. R., Gochis, D. J., and Mascaro, G.: On the diurnal cycle of surface energy fluxes in the North American monsoon region using the WRF-Hydro modeling system, Journal of Geophysical Research: Atmospheres, 122, 9024–9049, https://doi.org/10.1002/2017JD026472, 2017.

https://doi.org/10.5194/egusphere-2023-835
Preprint. Discussion started: 24 May 2023

Appendix A: Internal ice temperatures from oldrunoff_oldalbedo and newrunoff_oldalbedo

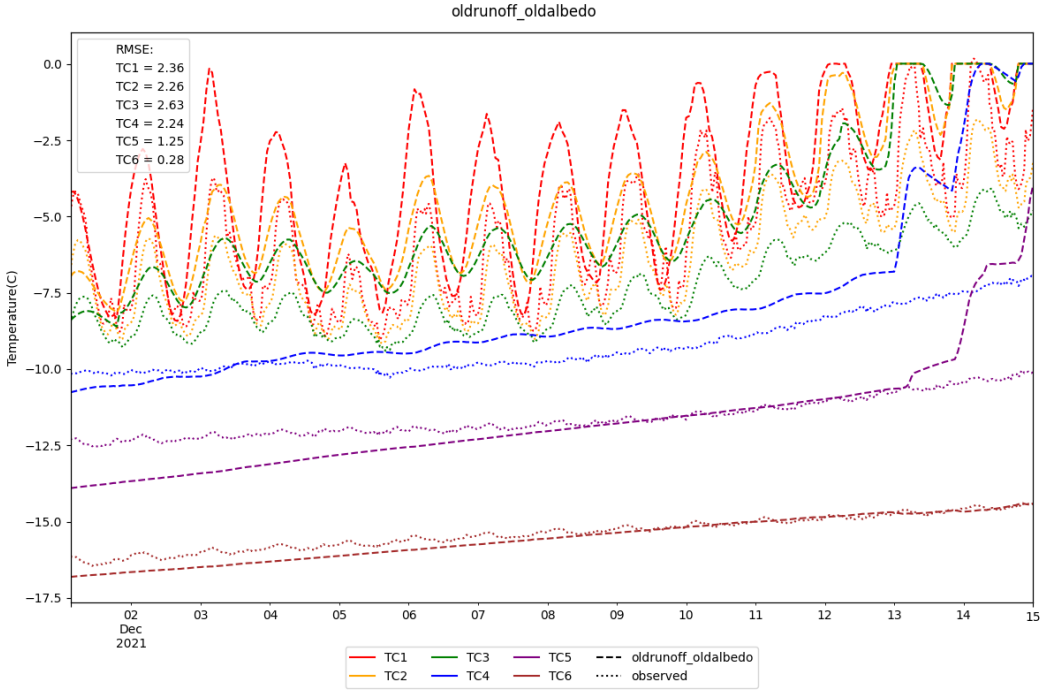

Figure A1. Modelled internal ice temperatures from oldrunoff_oldalbedo over the first two weeks of December. Thermocouples were initially deployed at six different depths: 0.05, 0.1, 0.2, 0.5, 1.0 and 2.0 meters. Note that the measurements are not at a constant depth with time as the sensors were melting out over the period.

https://doi.org/10.5194/egusphere-2023-835
Preprint. Discussion started: 24 May 2023

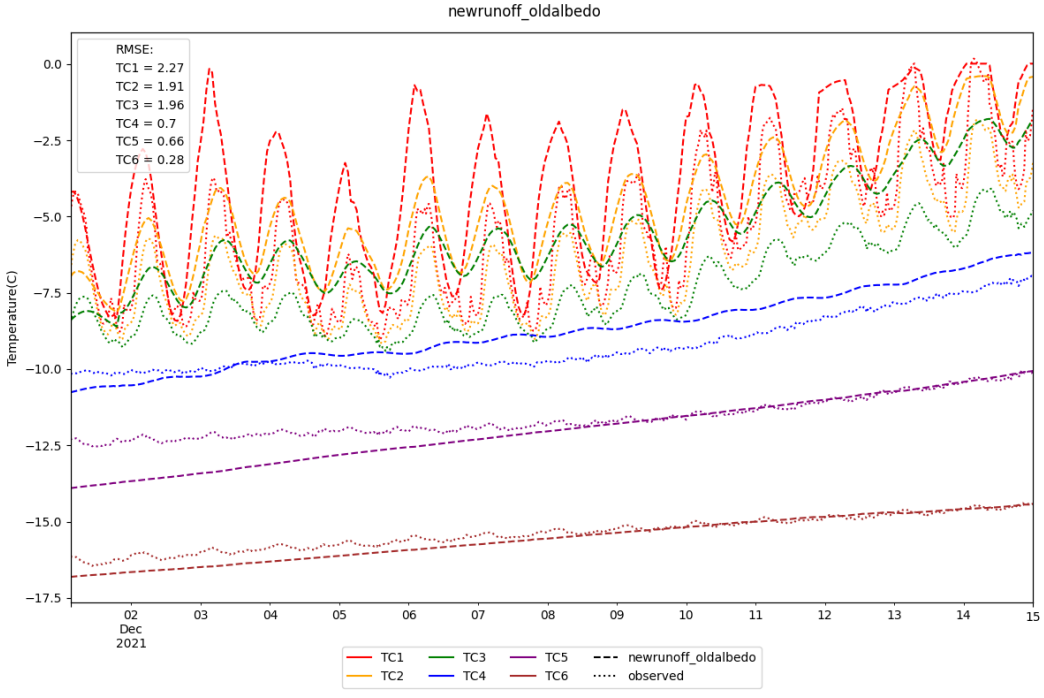

Figure A2. Modelled internal ice temperatures from newrunoff_oldalbedo over the first two weeks of December. Thermocouples were initially deployed at six different depths: 0.05, 0.1, 0.2, 0.5, 1.0 and 2.0 meters. Note that the measurements are not at a constant depth with time as the sensors were melting out over the period.